Optimisation of Geometric and Operational Conditions of a Flywheel Energy Storage System to Minimise Standby Losses

Mahmoud Eltaweel and Mohammad Reza Herfatmanesh

School of Physics, Engineering and Computer Science, University of Hertfordshire

ABSTRACT

Flywheel energy storage systems (FESSs) have gained significant attention as a promising technology for effective harvesting, storage and redeployment of energy. This technology is used particularly in renewable energy applications where they help manage the intermittency and variability of energy output from renewable sources such as solar and wind by providing quick response, high power density, and cycling stability without the degradation issues associated with chemical batteries. This paper presents a comprehensive study on the optimisation of geometric and operational conditions of a FESS, with the view to reduce standby losses hence improving the overall efficiency of the system. The effects of the following parameters are investigated; the working fluid, operating pressure and geometrical configuration of the FESS casing, using Computational Fluid Dynamics (CFD) simulations to provide insights into the system performance characteristics. This study investigates the effects of concave and convex casing shapes compared to conventional uniform cylindrical casings. The use of these distinct shapes can lead to lower standby losses. In addition, the effects of the working fluid and the operating pressure are investigated. The effects of different working fluids including air, helium and carbon dioxide, on standby losses are studied at different operating pressures. The findings of this study highlight the significant potential for improving FESS efficiency through the optimisation of FESS casing design and the use of a suitable working fluid at optimal operating pressure. Windage losses can be reduced by 90% compared to the base model, allowing the FESS to function as a medium-duration storage solution rather than a short-duration, which is often a limiting factor when considering FESSs as an alternative solution to battery storage systems.

Keywords: Energy storage, Flywheel energy storage system, Windage loss, Heat transfer, Response surface method, Computational fluid dynamics.

NOMENCLATURE

C_m	Disk torque coefficient
C_w	Rotor skin friction coefficient
r_h	Internal housing radius
r_o	Rotor radius
$\nabla \cdot \tau_{ij}$	Viscous force
∇p	Pressure force
g	Airgap width
L	Rotor length
n	Number of responses
T	Temperature
V	Velocity vector
Γ	Aspect ratio
η	Radius ratio
λ	Thermal conductivity
ρ	Density
ρg	Gravitational force
Φ	Heat from the conversion of mechanical energy
ω	Rotational velocity

1. INTRODUCTION

Energy storage technology evolution has become an integral component in the pursuit of sustainable energy solutions. Among these technologies, Flywheel Energy Storage Systems (FESSs) have emerged as a robust contender, especially in the realm of renewable energy applications [1]. FESS offers a compelling solution to the challenges of intermittency and variability of energy output inherent in renewable energy sources such as solar and wind [2]. FESSs offer rapid response, high power density, and cycling stability, while

avoiding the degradation issues prevalent in chemical batteries, thus they have become an enabling technology in modern energy systems [3].

FESSs employ the principles of rotational kinetic energy storage, offering a reliable and high-efficiency method for energy storage and retrieval [4]. A flywheel rotor is a mechanical component with a specific mass that rotates at a particular speed, storing kinetic energy due to the rotation of the flywheel around its axis[5]. Advancements in technology have driven efforts to both enhance the operational capabilities and improve the performance of FESS [6]. A primary challenge in optimising FESSs is reducing windage losses [7]. These losses occur due to friction between the flywheel rotor and the working fluid, leading to energy dissipation in the form of heat [8]. In high-speed rotating devices such as flywheels, windage losses are a major contributor to total losses, heightening self-discharge and consequently diminishing their efficiency and efficacy [7]. Consequently, windage losses can potentially limit the suitability of FESSs for medium-duration energy storage applications [9].

A typical FESS is composed of an outer fixed cylinder and an inner rotating cylinder, which results in the formation of Taylor-Couette flow with the FESS annulus. In this arrangement, Taylor vortices form once the rotation speed surpasses a specific limit, consequently influencing the flow dynamics of the system [10].

Optimisation of a FESS involves careful consideration of various design parameters to minimise energy loss and enhance system performance. The intensity of the windage loss is a function of the flywheel speed, airgap size and operating pressure. The size of the airgap is an important factor when designing a FESS. In their pursuit of reducing windage losses, researchers Nakane [11] and Pfister [12] have proposed methods and models to lower windage losses in high-speed applications, reporting that certain configurations, such as the inclusion of rotor shrouds or adjusting the airgap size, can lead to improved torque and power efficiency. Awad and Martin [13] investigated windage losses on both the disc and cylinder sides of pulse generator rotors. For the disc and cylinder sides, the skin friction coefficient is a function of the Taylor number.

Reduction of working pressure (i.e. Partial vacuum) can also reduce windage losses since there will be fewer air molecules to create friction and drag [9]. Another method of reducing windage losses is to use a working fluid with lower density than air [14], [15]. Investigations by Liu et al. [16] into various vacuum levels demonstrated the impact on windage heating within a high-speed flywheel. An innovative approach to further reduce aerodynamic losses involves using a helium-air mixture, as studied by Suzuki et al. [14], who found that a 50% helium mixture could lower losses by 43%, with greater reductions at higher helium concentrations.

Building on the versatility of Response Surface Methodology (RSM) in experimental and numerical analysis and optimisation studies, several investigations have highlighted its applications across different domains. Eiamsa-ard and Promvonge [17] demonstrated the utility of RSM in complex experimental analysis. Salviano et al. [18] applied it to enhance the heat transfer performance of plate-fin heat exchangers, while Nouri-borujerdi and Nakhchi [19] used RSM to identify key design parameters in annular flows. Lastly, Sun et al. [20] optimised Taylor-Couette flow using RSM, reporting that increased Reynolds numbers and slit widths significantly improved heat transfer.

This work presents a focused study on optimising the geometry and operational conditions of a FESS to reduce standby losses and improve system performance. It investigates the effects of various factors including working fluid, operating pressure and casing design, using Computational Fluid Dynamics (CFD) simulations. The primary objective of this research is to compare traditional cylindrical casings against novel concave and convex shapes to evaluate their impact on FESS performance. Additionally, the study examines the role of different working fluids (Air, helium and carbon dioxide) and operating pressures in reducing windage losses. Utilising RSM, the paper conducts numerical simulations and data analysis to elucidate the influence of housing design on flow field distribution and windage losses. This research is among the first to assess and report on the effects of concave and convex housing designs on FESS performance, offering insights that could enhance the design of similar rotational machinery.

The novelty of this research lies in its comprehensive examination of the aerodynamic optimisation of FESS to minimise standby losses. It pioneers the assessment and application of concave and convex housing designs on FESS performance, offering novel insights that could significantly enhance the design of rotational machinery. This study is distinctive in its use of CFD simulations to explore the effects of various working fluids and operating pressures, alongside innovative casing shapes, to reduce windage losses, marking a significant advancement in FESS efficiency optimisation.

2. NUMERICAL MODELLING

2.1 Governing equations and assumptions

The objective of this investigation is to formulate a numerical representation of a FESS featuring a streamlined, constricted and sealed airgap architecture. The CFD methodology is employed to predict variables such as skin friction coefficient, disc torque and heat transfer coefficient through the simulation of the airgap flow dynamics. The governing equations for the CFD code are predicated upon the conservation laws pertaining to fluid mechanics [21].

For this study, a computational domain specific to an enclosed FESS is constructed. This domain is subsequently subdivided into computational cells and nodal points. Upon mesh generation, the governing equations are discretised numerically into a set of linear algebraic equations via a finite volume technique [22]. The conservation of mass in fluid flow is articulated by the continuity equation, as delineated in Equation (1) [21].

$$\frac{\partial \rho}{\partial t} + \nabla . \rho V = 0 \quad (1)$$

Newton's second law postulates that the rate of momentum change in a fluid particle is equivalent to the aggregate forces acting upon said particle, as depicted in Equation (2) [23].

$$\frac{D(\rho V)}{Dt} = -\nabla p + \nabla \cdot \tau_{ij} + \rho g \quad (2)$$

Equation (3) provides the foundation for deriving the energy equation pertinent to a compressible and viscous Newtonian fluid flow [23].

$$\frac{D(\rho C_p T)}{Dt} = \nabla \cdot (\lambda \nabla T) + \Phi \quad (3)$$

where V is the velocity vector, ∇p is the pressure force, $\nabla \cdot \tau_{ij}$ is the viscous force, ρg is the gravitational force, $\nabla \cdot (\lambda \nabla T)$ is the heat conduction through the fluid element boundaries, λ is the thermal conductivity, T is the temperature and Φ is the heat from the conversion of mechanical energy.

The flow regime is defined by the Knudsen number, for values below 0.01 the Navier-Stokes equations apply, assuming a continuous and linearly viscous fluid [24]. In a FESS, windage losses occur due to viscous friction between the rotor and the working fluid in the airgap. These losses are influenced by the working fluid's velocity field, affected by tangential flow and Taylor-Couette effects. Windage losses can be quantified by analysing airgap flow dynamics, with Equation (4) providing a formula to calculate the power required to offset these losses [16].

$$P_w = \pi \rho \omega^3 {r_o}^4 L C_w + \rho \omega^3 {r_o}^5 C_m \quad (4)$$

where ω is the rotational velocity of the rotor, ρ is the fluid density, L is the rotor length, r_o is the rotor radius, C_w is the rotor skin friction coefficient, and C_m is the disk torque coefficient.

2.2 Mesh generation and boundary conditions

This study used ANSYS Fluent 2022R1 to model a simplified FESS as shown in Figure 1 which serves as the baseline model. Dimensionless parameters are employed to characterise the airgap. Specifically, the radius ratio, denoted by $\eta = r_o/r_h$, serves to define the airgap, where r_o and r_h are the radii of the rotor and the housing, respectively. Additionally, the aspect ratio is defined as $\Gamma = L/g$, where L is the rotor length and g is the airgap width, calculated as $g = r_h - r_o$. The rotor radius and length were 0.13m, with a 0.96 radius ratio leading to an airgap size of 5.4mm and an aspect ratio of 24. Periodic conditions were applied to simulate the flow within the FESS, reducing the model to an 8° segment for computational efficiency. Figure 2 shows three different housing designs employed in this study with top and side housing wall curvatures.

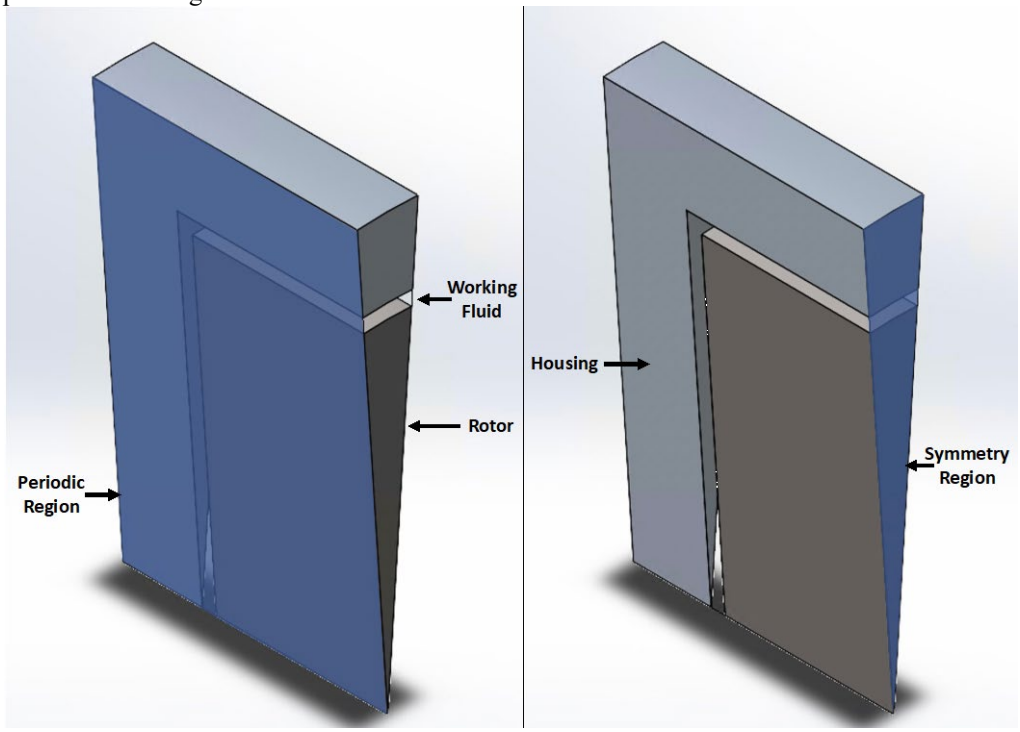

FIGURE 1: FESS SIMPLIFIED GEOMETRY WITH PERIODIC REGIONS AND SYMMETRY PLANE

Mesh independence analysis serves as an imperative pre-processing step that underpins the precision and reliability of numerical simulations. In this study, a structured quadrilateral mesh was employed to model a system featuring rotor and housing mesh sizes varying between 1mm and 2mm, along with an airgap mesh size ranging from 0.1mm to 0.2mm. The primary objective was to identify an optimised mesh for the simulations, conducted by executing a mesh independence assessment at a peak rotational speed of 2400 rad/s. Key parameters under consideration for this assessment were skin friction coefficient and Nusselt number. The range for the total mesh elements investigated spanned from 1 million to 12 million. Subsequent to the evaluation of these mesh independence tests, a mesh architecture comprising 9 million elements was selected as it offered a balance between computational resource efficiency and accuracy. In the context of numerical investigations, a thorough selection of both mesh type and quality is crucial. In order to accurately delineate flow profiles within wall boundary layers, wall treatment models were implemented. A high-resolution boundary layer mesh was constructed, utilising the wall cell $y_+ \leq 1$ to resolve the viscous sub-layer effectively. Figure 3 illustrates the mesh configuration employed in this study.

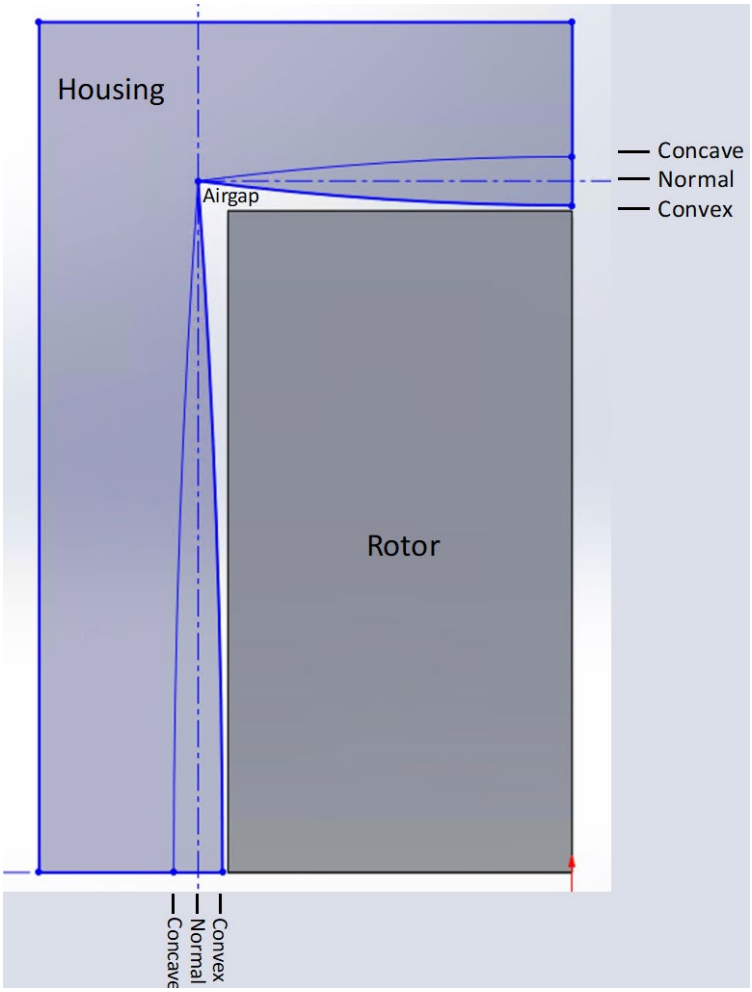

FIGURE 2: FLYWHEEL HOUSING WITH NORMAL, CONCAVE, AND CONVEX DESIGNS

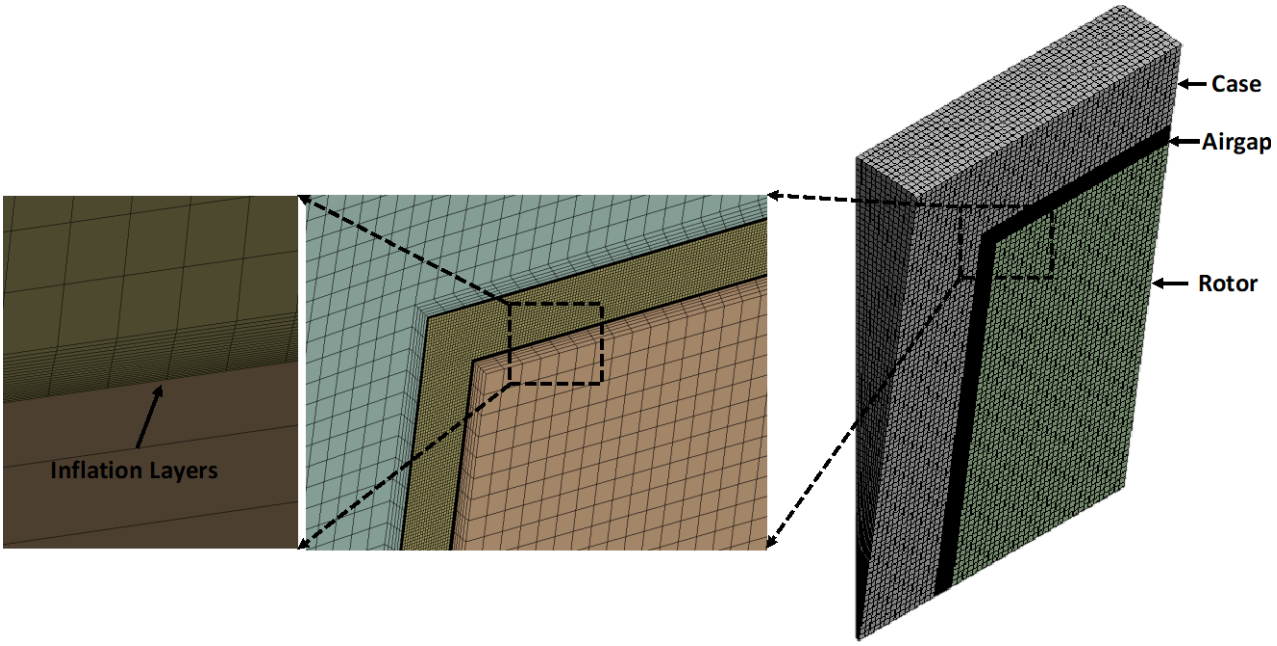

FIGURE 3: THE QUADRILATERAL MESH USED

To study the steady-state characteristics, a 3D steady-state turbulent flow model was employed. The time-averaged, steady-state solutions accounting for relative rotational motion were characterised by utilising a Moving Reference Frame (MRF) methodology. Within this framework, the rotor walls were modelled as moving walls, while the remaining components of the system were considered as stationary walls. This approach is well-suited for steady-state analysis and is capable of resolving a comprehensive range of flow parameters, including mass flow rates and pressure gradients across rotating elements [25].

Given that the Reynolds number within the airgap fell within the turbulent regime across all rotational speeds investigated, the incorporation of a turbulence model was requisite. Informed by a literature survey on turbulence modelling specifically for Taylor-Couette flow within concentric cylinders (Applicable to narrow-gap annuli with high-swirl rotational flow) the Reynolds-averaged Navier-Stokes (RANS) equations were solved utilising the k-ω SST turbulence model. This model has been empirically validated as efficacious for predicting fluid flow and heat transfer dynamics in concentric cylinder configurations [26], [27], [28], [29].

Several assumptions were made for the numerical analysis, including neglecting the effect of gravity, treating air as an ideal gas, and assuming thermal conductivity and specific heat to be constant. The system was modelled without an inlet or outlet. The thermal boundary condition applied to the housing included free stream temperature of 24°C and heat transfer coefficient of 30 W/m².K. All components were initially set to 24°C.

2.3 Numerical model validation

The oscillatory behaviour of skin friction coefficient as a function of Taylor number was examined in comparison with experimental data points, as documented by Donnelly [30]. In this comparison, the radius ratio was congruent with that of the CFD model.

Figure 4 outlines the skin friction coefficient and Taylor number distributions, illustrating three distinct flow regimes. The initial regime represents laminar flow devoid of vortices, followed by a second regime characterised by laminar flow with emergent Taylor-Couette vortices, termed as being congruent with non-linear theory owing to the non-linear distribution of skin friction coefficient. The final regime is turbulent flow featuring homogenously mixed. The numerically derived critical Taylor numbers align closely with literature-based propositions. Moreover, in instances where Taylor vortices manifest within the airgap, the skin friction coefficients deduced through CFD methodologies corroborate the empirical results obtained by Donnelly [30].

Empirical findings from the authors have further served to validate the CFD model [7]. Both experimental and numerical outcomes are in good agreement, exhibiting comparable flow behaviours, and the deviations between the two sets of data are confined within a 15% margin of error.

3. RESPONSE SURFACE METHODOLOGY

RSM is a statistical approach for exploring multifactorial tests with fewer trials. It is particularly effective in complex situations where multiple independent variables affect a dependent outcome. In this framework, Box-Behnken designs are crucial for creating higher-order response surfaces using fewer runs than traditional factorial methods. These designs include twelve mid-edge and three

central nodes in a cubic space, strategically positioned to enhance the statistical robustness of the analysis by fitting a quadratic model [17].

RSM is a precise and efficient tool for designing simulations and improving FESS performance. It is essential for understanding the impact of the housing design on vortex formation, flow field distribution and windage losses. RSM is key to identifying optimal operational parameters, enhancing efficiency and reliability in energy systems, highlighting its importance in fluid dynamics and energy optimisation.

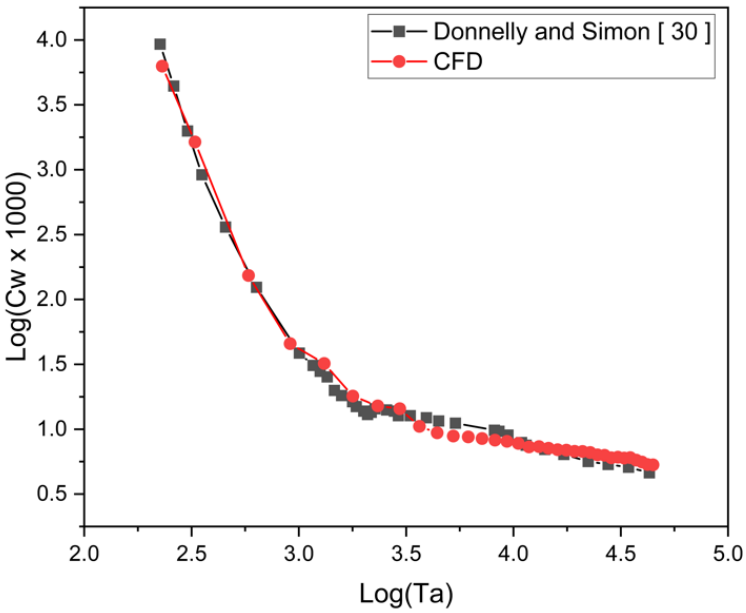

FIGURE 4: ROTOR SKIN FRICTION COEFFICIENT AS A FUNCTION OF TAYLOR NUMBER

3.1 Responses selection

The system responses are chosen to demonstrate the local form of the response surface by simulating the interaction and effects of the system parameters. They are also used to evaluate the strengths and weaknesses of a system to determine the best system settings. This model investigates windage losses which emerges as a determinant in quantifying the frictional losses within a FESS, having a direct influence on self-discharge rate of the system. The study aims to optimise the efficiency and energy conservation capabilities of FESSs by analysing windage losses in detail, highlighting critical areas for future research and development in flywheel-based energy storage systems.

3.2 Factors selection

The geometrical configuration of the inner surface of a FESS housing significantly impacts its performance. A curved FESS inner housing wall can significantly impact its performance and efficiency. A concave design augments the airgap in the central region, resulting in a decreased Taylor number which consequently affects skin friction coefficient. The reduction in Taylor number can lead to improved energy efficiency due to reduced frictional losses in the form of heat [31].

Additionally, exploring a convex shape forms part of a wider initiative to boost the aerodynamic efficiency of FESS. Convex geometries are recognised for enhancing heat dissipation due to a higher Taylor number and improved airflow dynamics, which also aids in aerodynamic drag reduction. The convex shapes promote a more laminar flow around the flywheel since the critical Taylor number is higher, delaying the formation of Taylor vortices and effectively reducing boundary layer thickness, thus, windage losses [32]. The primary goal is to strategically change the internal architecture of the casing to reduce windage losses.

Using a gas with lower density than air would result in less friction and drag, lowering windage losses [14], [15]. Other gases that could be used in the system besides air include Helium (He), a non-toxic, non-flammable, and inert gas less dense than air, resulting in less friction and drag. In addition, Helium's low viscosity and thermal conductivity can reduce heat loss and energy dissipation [14]. Another gas that can be used to reduce windage losses is hydrogen (H). It is also less dense than air, however, hydrogen is highly flammable and explosive, making it unsuitable for use in FESS not a practical option for [33].

On the other hand, Carbon dioxide (CO_2) is a colourless and odourless gas that is non-toxic and non-flammable, a more suitable option compared to hydrogen. The choice of CO_2, despite its higher density, is predicated on its superior thermodynamic properties, including a higher specific heat capacity and thermal conductivity. These characteristics are critical in mitigating thermal gradients and facilitating more efficient heat dissipation within the system. The use of CO_2 is intended to reduce windage losses through improved thermal regulation [34].

This study investigates a broad range of parameters influencing FESS performance including the working pressure, housing wall curvature and working fluid. The rotational velocity of the rotor is fixed at 2400 rad/s, which represents the maximum permissible speed for a solid steel cylindrical rotor with a safety factor of two [35]. Table 1 details the studied variables and their respective levels, expressed in both actual and coded values. The upper and lower limits of the factors are encoded as +1 and -1, respectively, with 0 representing the intermediate level [17].

4. RESULTS AND DISCUSSION

4.1 RSM response

Windage losses in a FESS are studied in detail through the application of Analysis of Variance (ANOVA) in this study. Table 2 lists significant factors influencing windage losses and their interactions. the model was statistically significant, as evidenced by F-values of 1687.64. Model terms with P-values less than 0.05 were considered significant, while those with P-values greater than 0.10 were considered insignificant. Certain responses were marked as significant, resulting in the exclusion of insignificant factors to improve the model's predictive accuracy. Furthermore, the F-values for individual factors and their interactions were computed to determine the significance of their mean square variations. Concurrently, relevant P-values were calculated using a 95% confidence interval. The statistical results validate the model's ability to predict windage losses within the numerical variable range. All the analysed factors are significant, except for the side curvature; this indicates that variations in the side curvature do not substantially impact windage losses.

In regression analysis, the mathematical model serves to articulate the correlation between input variables and dependent responses. The fit statistics for the preliminary response, exhibit a robust coefficient of determination (R^2) exceeding 0.99, signifying minimal discrepancy between the regression model and actual response data points. Furthermore, the adjusted R^2 value, refined to exclude insignificant parameters, remains superior to 0.998, underscoring minimal data variability. The model's predictive ability for new observations is evaluated via the predicted R^2 value. A marginal deviation of 0.2 from the adjusted R^2 underscores a praiseworthy model correlation.

TABLE 1: STUDIED VARIABLES AND THEIR LEVELS

Parameters	Levels		
	Lower level (-1)	Intermediate level (0)	Higher level (+1)
A: Top housing wall curvature (mm)	-4.4 (convex)	0	4.4 (concave)
B: Side housing wall curvature (mm)	-4.4 (convex)	0	4.4 (concave)
C: Working pressure (mbar)	100	550	1000
D: Working fluid	Helium	Air	Carbon Dioxide

4.2 Fluid flow characteristics

As the rotational velocity of a FESS increases, the Taylor-Couette vortices become more pronounced. These vortices arise due to the relative motion of the FESS rotor and housing. Their formation is influenced by various factors, including airgap size, rotational velocity and working fluid properties. At low rotational velocities, the Taylor-Couette vortices may be relatively weak and less pronounced; however, as the velocity increases, vortices become more turbulent and intense. This has several effects on the overall FESS performance, including increased windage losses.

One of the primary factors affecting the occurrence of Taylor vortices is the airgap size. A diminished airgap size is associated with a surge in the number of Taylor vortices, which in turn significantly impacts the skin friction coefficient, resulting in increased windage losses. Taylor vortices appear more frequently as the airgap size increases, while Taylor cells are less rapidly affected by azimuth waves as the airgap size reduces [36]. The curvature of the top housing wall significantly modulates Taylor-Couette vortex dynamics by altering the flow within the airgap. Variations in airgap size, achieved through modulation, directly influence the number of Taylor vortices, thereby offering a method to adjust the Taylor number according to the desired outcome. Specifically, null housing curvature yields 22 Taylor cells, while concave design results in 8 and convex configuration leads to 52 cells, as illustrated in Figure 5.

4.3 Windage losses

Windage losses arise from the viscous friction between the rotor and the surrounding fluid during a FESS rotation. Factors such as the rotational speed and thermo-physical properties of the working fluid play a significant role in determining these losses. An analysis has been conducted on the impact of rotational speed on windage losses across various scenarios. As the rotational speed escalates, there is an alteration in the velocity distribution within the airgap. This is attributed to the Taylor number surpassing its critical threshold of 41.3, resulting in the formation of Taylor vortices.

TABLE 2: ANALYSIS OF VARIANCE FOR WINDAGE LOSSES

Source	Sum of Squares	df	Mean Square	F-value	p-value
A-Top housing wall curvature	49.22	1	49.22	226.95	< 0.0001
B-Side housing wall curvature	0.0381	1	0.0381	0.1758	0.6787
C-Working pressure	2832.30	1	2832.30	13058.45	< 0.0001
D-Working fluid	3922.66	2	1961.33	9042.80	< 0.0001
AD	1.99	2	0.9973	4.60	0.0204
BD	0.0292	2	0.0146	0.0673	0.9351
CD	343.53	2	171.77	791.93	< 0.0001
Lack of fit	5.21	18	0.2892		
Pure error	0	6	0		
Total	7325.98	44			

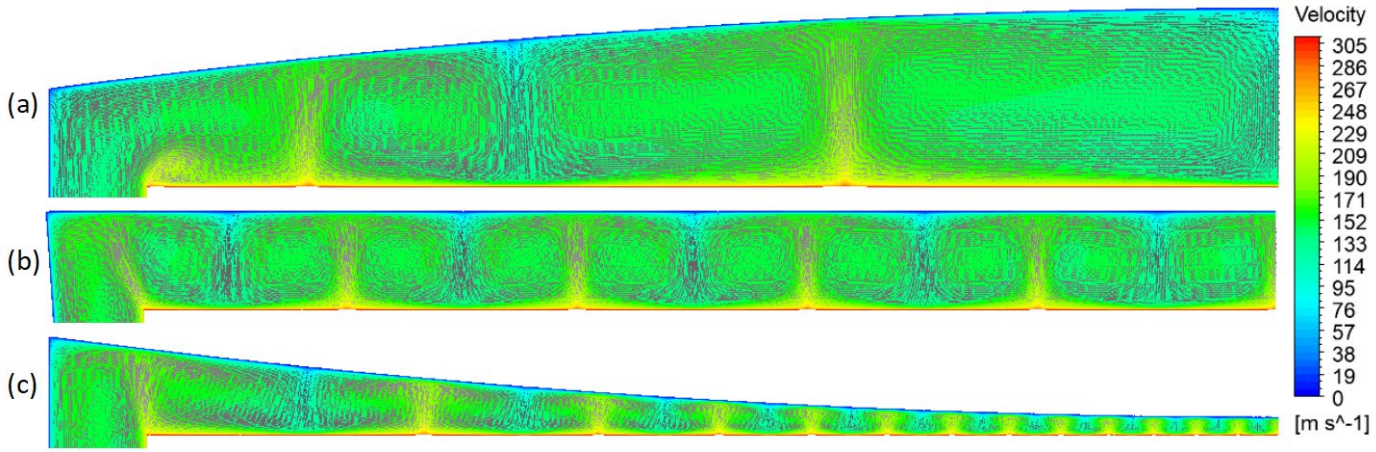

FIGURE 5: VELOCITY CONTOUR WITHIN THE AIRGAP AT 1 BAR PRESSURE WITH AIR AS WORKING FLUID FOR THE FOLLOWING TOP HOUSING WALL CURVATURE: (A) NORMAL, (B) CONCAVE, AND (C) CONVEX

Figure 6 illustrates the relationship between the windage losses of the studied FESS and the top and side housing wall curvatures. The graph presents a three-dimensional surface where the x-axis represents the curvature of the top housing wall, the y-axis represents the curvature of the side housing wall, and the z-axis indicates the resulting windage losses measured in watts. The curvatures vary from normal (i.e. Flat) to concave and convex. The range of curvature is symmetrically distributed around zero, the point of no curvature, extending to both positive and negative values indicating convex and concave shapes, respectively. The surface plot shows how windage losses change as the curvature of both housing parts changes. The aim of this analysis is to determine which housing curvature minimises windage losses. Reduced losses allow the system to achieve a lower rate of self-discharge, improving its overall efficiency.

The conditions under which this response is observed include operation at atmospheric pressure and the use of Helium, air and Carbon dioxide as the working fluid. In Figure 6(a), Helium serves as the working fluid due to its low density, thereby potentially reducing windage losses compared to denser fluids. Variations in the side housing wall curvature from concave to convex do not noticeably influence windage losses. However, the top housing wall curvature does impact windage losses, with the concave shape mitigating windage losses more effectively than the convex configuration.

Figure 6(b) demonstrates the impact of air as a working fluid. The green surface plot indicates that when air is used as the working medium, the windage losses are higher compared to helium, due to higher density of air causing greater frictional losses. The plot also highlights that the top housing wall curvature has a more significant influence on reducing windage losses compared to the side housing wall curvature. From concave to convex, the side housing wall curvature does show a trend towards reducing windage losses, but this effect is less pronounced than that of the top housing wall curvature.

Figure 6(c) illustrates the impact of carbon dioxide (CO2) as a working fluid. The plot shows that windage losses are highest when CO2 is used as the working medium, surpassing those observed with air and helium. This is attributed to the higher density of CO2 compared to the other working fluids, which leads to increased frictional losses. The top housing wall curvature continues to show a significant impact on windage losses, more so than the other two working fluids. The side housing wall curvature, on the other hand, suggests that a normal, non-curved, configuration is most beneficial in minimising windage losses when CO2 is used.

Figure 7 provides an analysis of the windage losses based on the interplay between the top housing wall curvature and the operating pressure, with a fixed, normal side housing wall. There is a direct correlation between pressure and windage losses. For all working fluids studied, the windage losses decrease as the working pressure is reduced. The top housing wall curvature has a variable impact on windage losses, which is more pronounced at higher pressures. At elevated pressures, the density of the working fluid increases, amplifying the effect of the curvature on windage losses due to the increased interaction between the fluid particles and the housing surfaces.

4.3 Optimisation

Myers and Montgomery [37] introduced the concept of "desirability" within the context of a multiple-response optimisation method. The desirability function, denoted as *D(X)*, serves as the objective function in this multi-criterion decision-making process. The function assigns a value within the range of zero to one to each response, where one indicates the highest desirability and zero represents conditions outside the desirable range. The composite objective function, which encapsulates the overall desirability, is constructed as the geometric mean of these individual transformed responses, as shown in Equation (5).

$$D = (d_1 \cdot d_2 \cdot \dots d_n)^{\frac{1}{n}} = (\prod_{i=1}^{n} d_i)^{\frac{1}{n}} \qquad (5)$$

where n is the number of responses measured and d_i is the desirable range for each response. This function transitions linearly from zero, outside the predetermined limits, to one at the target point. Numerical optimisation was employed to maximise a desirability function that considers a range of responses and variables, allowing for the weighting of each objective to tailor the outcome.

To reduce windage losses, the optimal configuration was found with top and side housing wall curvatures set to -2.2mm and -2.3mm, respectively, coupled with an internal pressure of 100mbar and helium as the working fluid, achieving a complete desirability score of 1. However, employing helium and a partial vacuum introduces additional design complexities. An alternative solution, which simplifies the previous design by operating at atmospheric pressure, suggests setting the top and side housing wall curvatures to -4.4mm and 0mm, respectively. This setup achieved a desirability score of 0.84. In comparison to the standard design, which features a normal housing wall and uses air at atmospheric pressure, the windage losses were reduced by 91% in the first optimisation scenario and by 75% in the second, marking significant improvements compared to the baseline model.

Minimising windage losses has a notable impact on standby losses, which in turn influences the self-discharge rate of the system. With the maximum rotational velocity of the studied FESS set at 2400 rad/s, equating to a full state of charge (SOC), and the minimum velocity of 600 rad/s, corresponding to a SOC of zero, Figure 8 contrasts the SOC over time between the baseline model and the two optimised models. The base model, when fully charged, experiences complete discharge due to mechanical losses (windage and bearing losses) within 43 minutes. In contrast, the second optimised system, utilising helium at atmospheric pressure, extends this duration by approximately threefold. Finally, the first optimised model further prolongs this timeframe to approximately seven times that of the base model, enabling the FESS to function as a medium-duration storage solution rather than being limited to short-duration applications.

Li et al. [38] showed that integrating a FESS with a PV system could boost its self-sufficiency from 36.8% to 51.9%, and the self-consumption rate from 30.2% to 61.4%. However, since the flywheel is either fully charged or idle 67% of the time, it suffers from standby losses, notably during extended periods of inactivity at maximum speed, limiting its energy efficiency to about 40%. This is significantly less than the efficiencies of lead-acid (70%-84%) and Li-ion batteries (85%-95%). Reducing these standby losses could make FESS more competitive against traditional battery technologies.

Integrating a FESS with a PV system and achieving longer discharge times due to reduced windage losses directly enhances the overall performance of a PV system. This improvement allows the system to store solar energy more efficiently during periods of peak sunlight and release it over extended durations, especially during low light conditions or at night. Consequently, such PV systems can maintain a more consistent power supply, reducing reliance on external power sources thus improving energy self-sufficiency. Extending the discharge time from 43 minutes to over 340 minutes can potentially triple the usable energy output during peak demand times or low solar production periods, significantly enhancing PV systems' reliability and reducing the need for supplementary energy sources.

Table 3 compares the findings of the current study with those reported by Suzuki et al. [14] and Ajisman et al. [15], focusing on the reduction of windage losses in FESS through various methods. The markedly higher reduction percentages achieved in this study suggests a potentially novel approach to aerodynamic optimisation.

5. CONCLUSION

This study has explored the aerodynamic optimisation of a FESS to mitigate standby losses. The study incorporated a multi-faceted approach, examining the interplay between FESS housing wall curvature, operating pressure, and working fluid, with a focus on minimising windage losses. The findings illustrate:

- The appropriate choice of working fluid, particularly the use of helium, coupled with the optimised geometrical configuration of the FESS housing, can significantly reduce aerodynamic losses due to friction.
- The use of numerical optimisation techniques has provided multiple viable solutions, facilitating a balance between system complexity and efficiency.
- The key finding of this study is the determination of an optimal top and side housing wall curvatures at reduced working pressures which markedly enhance the system performance.
- The findings of this study demonstrate that FESSs have the potential to serve as a medium-duration energy storage solution rather than being limited to short-duration applications.

Furthermore, the comparative analysis of different working fluids under different operating pressures has offered valuable insights into the scalability and adaptability of FESS designs under diverse operational conditions. The research emphasises the potential of FESS in the broader context of energy storage for renewable energy sources such as solar and wind, underscoring the necessity for continued innovation in this field. The implications of this research are significant, offering a pathway to more sustainable and efficient energy storage solutions. As the demand for renewable energy integration increases, the findings from this study can provide a crucial foundation for the design and development of next-generation FESS units that are not only cost-effective but also exhibit enhanced performance and reliability.

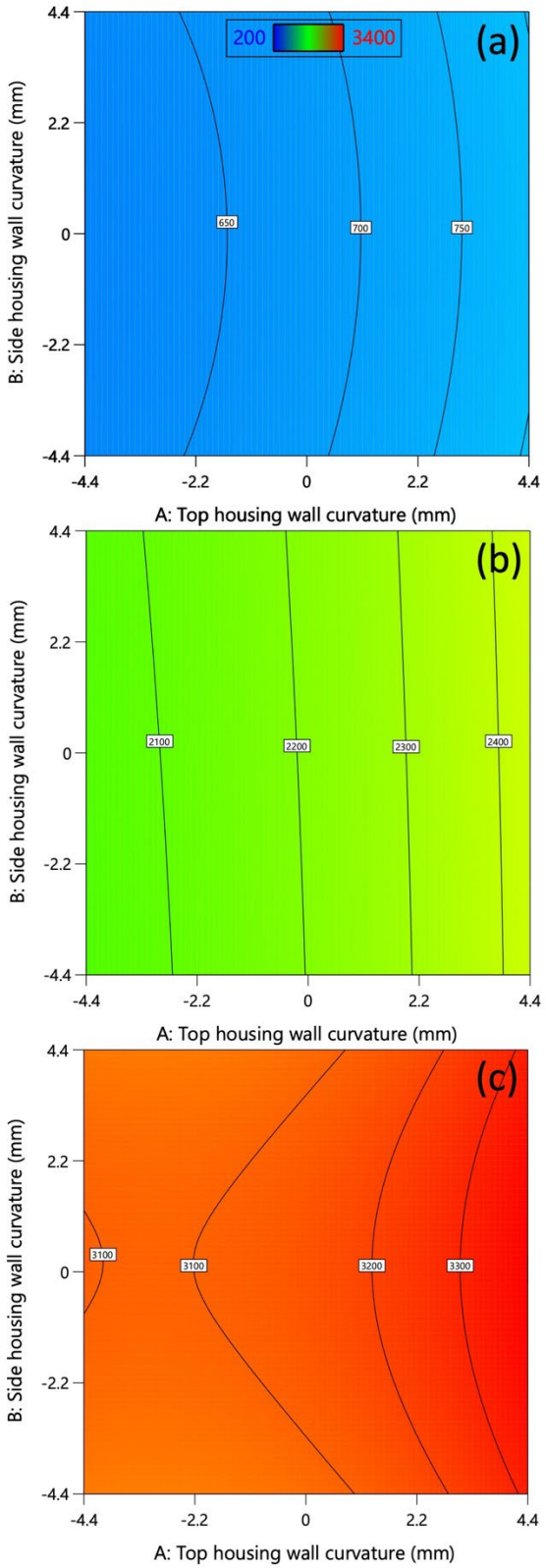

FIGURE 6: 3D PLOT OF WINDAGE LOSSES IN A FESS AS A FUNCTION OF TOP AND SIDE HOUSING WALL CURVATURES AT 1 BAR PRESSURE FOR THE FOLLOWING WORKING FLUIDS: (A) HELIUM, (B) AIR, AND (C) CARBON DIOXIDE

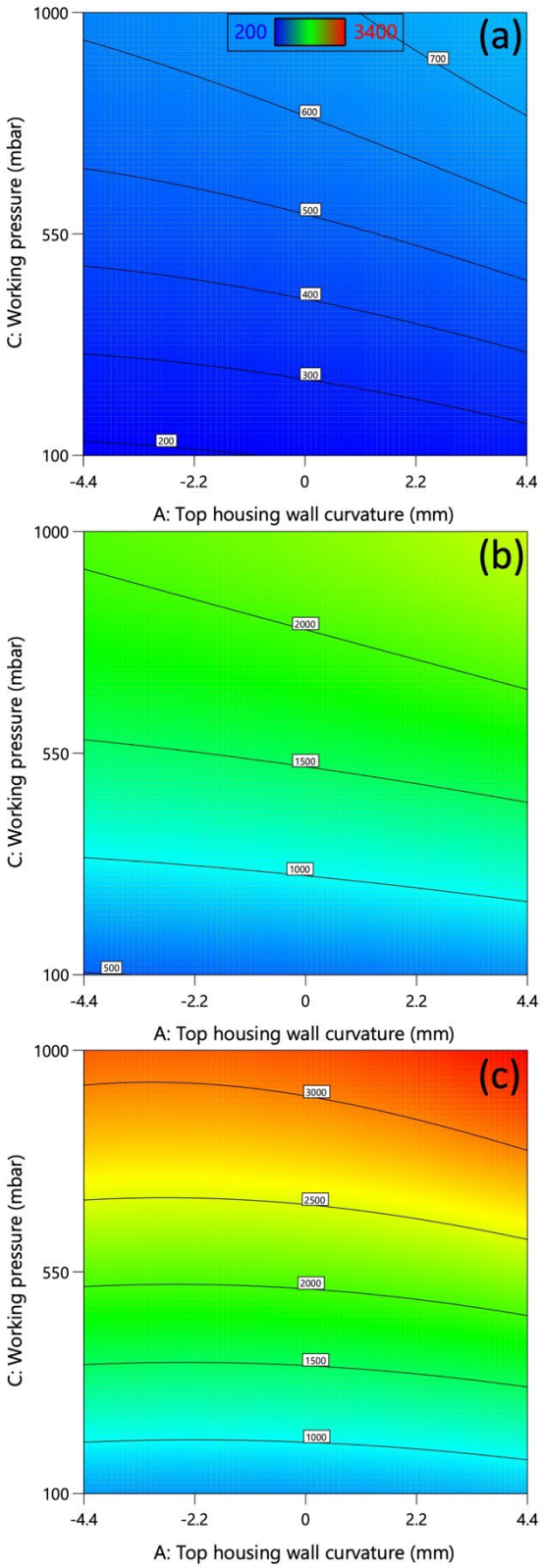

FIGURE 7: 3D PLOT OF WINDAGE LOSSES IN A FESS AS A FUNCTION OF TOP HOUSING WALL CURVATURE AND PRESSURE FOR THE FOLLOWING WORKING FLUIDS: (A) HELIUM, (B) AIR, AND (C) CARBON DIOXIDE

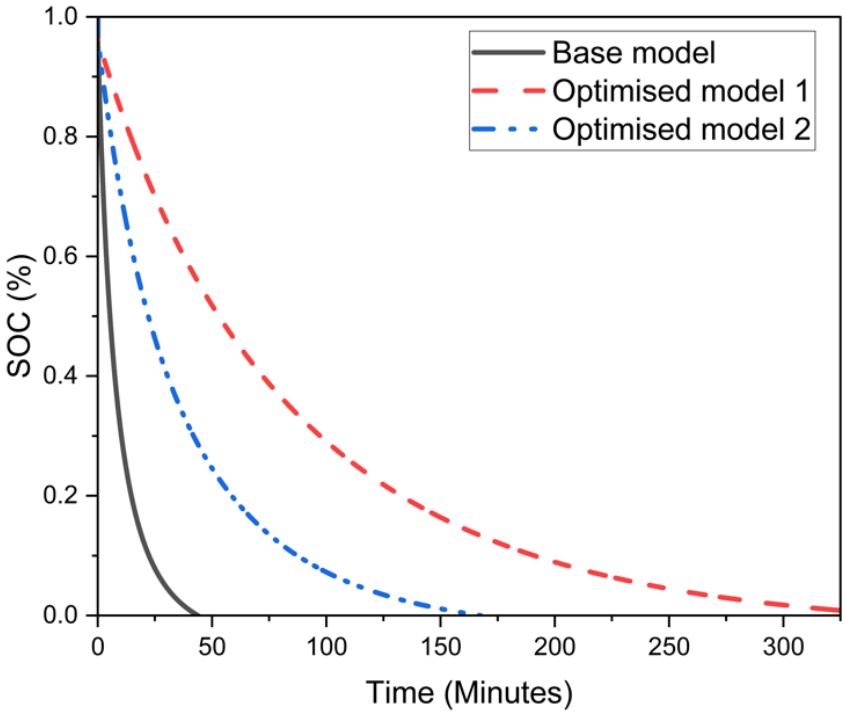

FIGURE 8: FESS STATE OF CHARGE OVER TIME FOR THE BASE MODEL AND THE TWO OPTIMISED MODELS

TABLE 3: COMPARISON OF WINDAGE LOSS REDUCTION FOR THE CURRENT STUDY AND PREVIOUS RESEARCH

Reference	Reduction in Windage Losses	Modification
Current Study	91%	• 100 vol% Helium • Novel casing design • Partial vacuum
	75%	• 100 vol% Helium • Novel casing design
Eltaweel and Herfatmanesh [39]	64%	• Partial vacuum • Slit walls inside the casing
Suzuki et al. [14]	43%	• 50 vol% Helium / Air
	70%	• 75 vol% Helium / Air
Ajisman et al. [15]	42%	• 50% Helium / 50% Air

ACKNOWLEDGEMENTS

This work is supported by the European Union's Horizon 2020 research and innovation programme under the Marie Skłodowska-Curie grant agreement No 801604.

REFERENCES

[1] E. Hossain, H. M. R. Faruque, M. S. H. Sunny, N. Mohammad, and N. Nawar, 'A comprehensive review on energy storage systems: Types, comparison, current scenario, applications, barriers, and potential solutions, policies, and future prospects', *Energies*, vol. 13, no. 14, p. 3651, 2020.

[2] P. Das, J. Mathur, R. Bhakar, and A. Kanudia, 'Implications of short-term renewable energy resource intermittency in long-term power system planning', *Energy Strategy Rev.*, vol. 22, pp. 1–15, 2018.

[3] M. E. Amiryar and K. R. Pullen, 'A review of flywheel energy storage system technologies and their applications', *Appl. Sci.*, vol. 7, no. 3, p. 286, 2017.

[4] A. G. Olabi, T. Wilberforce, M. A. Abdelkareem, and M. Ramadan, 'Critical review of flywheel energy storage system', *Energies*, vol. 14, no. 8, p. 2159, 2021.

[5] G. Genta, *Kinetic energy storage: theory and practice of advanced flywheel systems*. Butterworth-Heinemann, 1985.

[6] X. Li and A. Palazzolo, 'A review of flywheel energy storage systems: state of the art and opportunities', *J. Energy Storage*, vol. 46, p. 103576, 2022.

[7] S. Motaman, M. Eltaweel, M. R. Herfatmanesh, T. Knichel, and A. Deakin, ‘Numerical analysis of a flywheel energy storage system for low carbon powertrain applications’, *J. Energy Storage*, vol. 61, p. 106808, May 2023, doi: 10.1016/j.est.2023.106808.
[8] E. Gundabattini, R. Kuppan, D. G. Solomon, A. Kalam, D. Kothari, and R. A. Bakar, ‘A review on methods of finding losses and cooling methods to increase efficiency of electric machines’, *Ain Shams Eng. J.*, vol. 12, no. 1, pp. 497–505, 2021.
[9] M. E. Amiryar and K. R. Pullen, ‘Analysis of standby losses and charging cycles in flywheel energy storage systems’, *Energies*, vol. 13, no. 17, p. 4441, 2020.
[10] A. Nouri-Borujerdi and M. Nakhchi, ‘Heat transfer enhancement in annular flow with outer grooved cylinder and rotating inner cylinder: Review and experiments’, *Appl. Therm. Eng.*, vol. 120, pp. 257–268, 2017.
[11] H. Nakane, Y. Okada, T. Kosaka, and N. Matsui, ‘Experimental study on windage loss reduction using two types of rotor for hybrid excitation flux switching motor’, presented at the 2016 XXII International Conference on Electrical Machines (ICEM), IEEE, 2016, pp. 1707–1713.
[12] P.-D. Pfister and Y. Perriard, ‘A 200 000 rpm, 2 kW slotless permanent magnet motor’, presented at the 2008 International Conference on Electrical Machines and Systems, IEEE, 2008, pp. 3054–3059.
[13] M. Awad and W. Martin, ‘Windage loss reduction study for TFTR pulse generator’, presented at the 17th IEEE/NPSS Symposium Fusion Engineering (Cat. No. 97CH36131), IEEE, 1997, pp. 1125–1128.
[14] Y. Suzuki, A. Koyanagi, M. Kobayashi, and R. Shimada, ‘Novel applications of the flywheel energy storage system’, *Energy*, vol. 30, no. 11–12, pp. 2128–2143, 2005.
[15] K. Yamagata, J. Kobuchi, and R. Shimada, ‘Study of cooling gases for windage loss reduction’, *IEEJ Trans. Power Energy*, vol. 120, no. 3, pp. 478–483, 2000.
[16] H.-P. Liu, M. Werst, J. J. Hahne, and D. Bogard, ‘Prediction of windage losses of an enclosed high speed composite rotor in low air pressure environments’, presented at the Heat Transfer Summer Conference, 2003, pp. 15–23.
[17] A. Nouri-Borujerdi, M. Bovand, S. Rashidi, and K. Dincer, ‘Geometric parameters and response surface methodology on cooling performance of vortex tubes’, *Int. J. Sustain. Energy*, vol. 36, no. 9, pp. 872–886, Oct. 2017, doi: 10.1080/14786451.2015.1127233.
[18] L. O. Salviano, D. J. Dezan, and J. I. Yanagihara, ‘Optimization of winglet-type vortex generator positions and angles in plate-fin compact heat exchanger: response surface methodology and direct optimization’, *Int. J. Heat Mass Transf.*, vol. 82, pp. 373–387, 2015.
[19] A. Nouri-Borujerdi and M. Nakhchi, ‘Optimization of the heat transfer coefficient and pressure drop of Taylor-Couette-Poiseuille flows between an inner rotating cylinder and an outer grooved stationary cylinder’, *Int. J. Heat Mass Transf.*, vol. 108, pp. 1449–1459, 2017.
[20] S. Sun, D. Liu, W.-D. Shi, Y.-Z. Wang, and H.-B. Kim, ‘Numerical Simulations of Heat Transfer Performance of Taylor–Couette Flow in Slit Model’, *Arab. J. Sci. Eng.*, vol. 46, pp. 7153–7170, 2021.
[21] B. Andersson, R. Andersson, L. Håkansson, M. Mortensen, R. Sudiyo, and B. Van Wachem, *Computational fluid dynamics for engineers*. Cambridge university press, 2011.
[22] N. Regalado-Rodríguez and C. Militello, ‘Comparative study of the effects of increasing heat transfer area within compression and expansion chambers in combination with modified pistons in Stirling engines. A simulation approach based on CFD and a numerical thermodynamic model’, *Energy Convers. Manag.*, vol. 268, p. 115930, 2022.
[23] J. Tu, G. H. Yeoh, and C. Liu, ‘Chapter 3 - Governing Equations for CFD—Fundamentals’, in *Computational Fluid Dynamics*, J. Tu, G. H. Yeoh, and C. Liu, Eds., Burlington: Butterworth-Heinemann, 2008, pp. 65–125. doi: 10.1016/B978-075068563-4.50005-7.
[24] N. G. Hadjiconstantinou, ‘The limits of Navier-Stokes theory and kinetic extensions for describing small-scale gaseous hydrodynamics’, *Phys. Fluids*, vol. 18, no. 11, p. 111301, 2006.
[25] J. D. Anderson and J. Wendt, *Computational fluid dynamics*, vol. 206. Springer, 1995.
[26] C. Jungreuthmayer *et al.*, ‘A detailed heat and fluid flow analysis of an internal permanent magnet synchronous machine by means of computational fluid dynamics’, *IEEE Trans. Ind. Electron.*, vol. 59, no. 12, pp. 4568–4578, 2011.
[27] K. R. Anderson, J. Lin, C. McNamara, and V. Magri, ‘CFD study of forced air cooling and windage losses in a high speed electric motor’, *J. Electron. Cool. Therm. Control*, vol. 5, no. 02, p. 27, 2015.
[28] A. Nachouane, A. Abdelli, G. Friedrich, and S. Vivier, ‘Estimation of windage losses inside very narrow air gaps of high speed electrical machines without an internal ventilation using CFD methods’, presented at the 2016 XXII International Conference on Electrical Machines (ICEM), IEEE, 2016, pp. 2704–2710.
[29] D. A. Howey, A. S. Holmes, and K. R. Pullen, ‘Measurement and CFD prediction of heat transfer in air-cooled disc-type electrical machines’, *IEEE Trans. Ind. Appl.*, vol. 47, no. 4, pp. 1716–1723, 2011.

[30] R. Donnelly, ‘Experiments on the stability of viscous flow between rotating cylinders I. Torque measurements’, *Proc. R. Soc. Lond. Ser. Math. Phys. Sci.*, vol. 246, no. 1246, pp. 312–325, 1958.
[31] R. Maryami, S. Farahat, M. JavadPour, and M. Shafiei Mayam, ‘Frictional drag reduction using small bubbles in a Couette-Taylor flow’, *J. Mar. Sci. Technol.*, vol. 20, pp. 652–669, 2015.
[32] V. Sinevic, R. Kuboi, and A. Nienow, ‘Power numbers, Taylor numbers and Taylor vortices in viscous Newtonian and non-Newtonian fluids’, *Chem. Eng. Sci.*, vol. 41, no. 11, pp. 2915–2923, 1986.
[33] J. Kobuchi, K. Oobayashi, and R. Shimada, ‘Windage loss reduction of flywheel/generator system using He and SF/sub 6/gas mixtures’, presented at the IECEC-97 Proceedings of the Thirty-Second Intersociety Energy Conversion Engineering Conference (Cat. No. 97CH6203), IEEE, 1997, pp. 1754–1757.
[34] L. Hu, Q. Deng, J. Li, and Z. Feng, ‘Model improvement for shaft-type windage loss with CO2’, *J. Supercrit. Fluids*, vol. 190, p. 105747, 2022.
[35] Y. Han, Z. Ren, and Y. Tong, ‘General Design Method of Flywheel Rotor for Energy Storage System’, *2012 Int. Conf. Future Energy Environ. Mater.*, vol. 16, pp. 359–364, Jan. 2012, doi: 10.1016/j.egypro.2012.01.059.
[36] M. Fénot, Y. Bertin, E. Dorignac, and G. Lalizel, ‘A review of heat transfer between concentric rotating cylinders with or without axial flow’, *Int. J. Therm. Sci.*, vol. 50, no. 7, pp. 1138–1155, 2011.
[37] R. H. Myers, D. C. Montgomery, and C. M. Anderson-Cook, *Response surface methodology: process and product optimization using designed experiments*. John Wiley & Sons, 2016.
[38] X. Li, N. Erd, and A. Binder, ‘Evaluation of flywheel energy storage systems for residential photovoltaic installations’, presented at the 2016 International symposium on power electronics, electrical drives, automation and motion (SPEEDAM), IEEE, 2016, pp. 255–260.
[39] M. Eltaweel and M. R. Herfatmanesh, ‘Numerical Investigation of Windage Loss and Heat Transfer in a High-Speed Flywheel Energy Storage System With Slit Wall’, presented at the Turbo Expo: Power for Land, Sea, and Air, American Society of Mechanical Engineers, 2023, p. V006T09A013.